# Sliding Mode Control of a Photovoltaic Based Shunt Active Power Filter in Islanding Operation

Fanjip René Constant[*] (iD), Kom Charles Hubert[‡**] (iD), Dzonde Naoussi Serge Raoul[***] (iD)

*Laboratory of Computer Science Engineering and Automation, Higher Normal School of Technical Education of Douala, University of Douala, Po Box 2701 Douala, Cameroon

**Laboratory of Energy, Materials, Modelling and Methods, National Higher Polytechnic School of Douala, University of Douala, Po Box 2701 Douala, Cameroon

***Laboratory of Technology and Applied Sciences, University Institute of Technology of Douala, University of Douala, Po Box 8698 Douala, Cameroon

(fangerene1@gmail.com, charleshubert.kom@gmail.com, serge.dzonde@univ-douala.com)

‡Corresponding Author; Po Box 2701 Douala, Cameroon, Tel: +237 696456745,

charleshubert.kom@gmail.com

**Abstract-** Renewable energy sources (RES) are constantly evolving nowadays due to the ever-increasing energy needs and the depletion of fossil fuel reserves. This, together with power quality problems, has led to the development of photovoltaic-based shunt active power filter (PV-SAPF) systems. However, the performance of these systems is linked to the control strategy used. Hence, to enable the PV system to perform the functions of power quality improvement, load supply, low THD current injection into the grid, and to avoid damage to connected loads during islanding operation, this paper proposes a control strategy for PV-SAPF in islanding operation. This control strategy is based on the optimal operating point tracking of the PV system. Multi-variable filter harmonic identification method is used for the determination of the harmonic and fundamental components of the reference currents of the grid-connected inverter. The islanding algorithm is used to detect a voluntary or involuntary disconnection from the grid. The performances of the proposed control strategy are evaluated for different operating scenarios by numerical simulations performed in MATLAB/Simulink software. The simulation results obtained show the good adaptation of the system in the different operating scenarios with harmonic distortion rates lower than the 5% recommended by the IEEE Std. 519-2014 standard, even during islanding. The responsiveness of the proposed control strategy is observed with the adaptation of the modulation coefficients of the fundamental components of the reference currents in the different operating modes.

**Keywords** Power quality problems; shunt active power filter; photovoltaic system; islanding operation; multi-variable filter.

| | | | |
|---|---|---|---|
| RES | Renewable Energy Sources | DC | Direct Current |
| GWdc | Giga Watt direct current | SAPF | Shunt Active Power Filter |
| PV | Photovoltaic | AC | Alternative Current |
| IEEE | Institute of Electrical and Electronics Engineers | PCC | Point of common Coupling |
| PV-SAPF | Photovoltaic-based Shunt Active Power Filter | SMC | Sliding Mode Controller |
| THD | Total Harmonic Distortion | | |
| MVF | Multi-Variable Filter | | |

## 1. Introduction

The demand for electrical energy from both household and industrial users is increasing, especially in developing countries [1]. This situation increases the already huge deficit between supply and demand, which is increasingly subject to environmental protection constraints [2]. The depletion of greenhouse gas emitting fossil fuels has forced governments to look at the energy potential of RES such as solar photovoltaic, wind turbine, fuel cells or biomass [3-4]. Among these RES, the development of the photovoltaic energy sector with 145 GWdc installed in 2020 [5], is a reason of the particular interest of researchers in this RES. Indeed, solar photovoltaic energy has great potential as an alternative energy resource to fossil fuels and is one of most promising due to energy free, clean, inexhaustible, easy conversion process, free-noise, sustainable and global availability [6-7]. Thus, for several decades, many works have been published on photovoltaic power generation [8-9], on low-THD current injection in grid-connected PV systems [10], parameters estimation of PV systems [11], optimal grid integration of PV systems [12], multi-source PV systems [13], maximum power point tracking [14] and power quality improvement [15].

Over the last decade, among these different applications of the PV system, power quality improvement is one of the most popular and promising concern. Indeed, the interconnection of the PV system via the power electronics converters to the grid must meet the requirements of the standard in terms of voltage magnitude, frequency and current harmonics. However, the dependence of the energy produced on weather conditions leads to the appearance of current and voltage harmonics in the grid [16]. In addition to the problem of harmonic currents injected by the PV system, the proliferation of power electronics-based equipment and non-linear loads connected to the grid that absorb no sinusoidal currents make harmonic currents a major power quality problem [17]. These harmonics are the cause of problems encountered by loads connected to the grid, such as disturbances in electronic equipment or motor malfunctions [18-20]. In order to eliminate harmonics and maintain power quality in the IEEE Std. 519-2014 [21], several solutions are recommended [22]. Traditional solutions mainly include shunt passive filters that are sized for a specific frequency [23]. Furthermore, the dynamic character of the harmonics constitutes a limit to the performances of the passive solutions. To avoid this limitation and eliminate random harmonic currents, modern solutions including mainly shunt active filters have been proposed [24-26]. In order to perform its power quality function, the PV system is combined with an active power filter. In this topology called photovoltaic-based shunt active power filter (PV-SAPF), the PV system performs with the load supply and low-THD current injection into the grid functions in addition to the power quality function [27-28].

In last decade, several control strategies have been proposed in literature for PV-SAPF system such as direct power control [29-30], instantaneous active and reactive powers theory [31-32], synchronous reference frame theory [33], artificial neural network [34-35], fuzzy logic [36-37] or model predictive control [38]. These control strategies use harmonic identification methods that depend on the grid voltage. This consideration is not a problem in the case where the grid is present and the results obtained in this work show this sufficiently. This study hypothesis takes us away from the reality of developing countries where a voluntary or accidental disconnection of the grid can occur, resulting in islanding operation. In such a scenario, the implementation of a control strategy that ensures the continuity of the load supply from the PV system is mandatory. Many researchers have studied this problem and have proposed several control strategies for this purpose. In [39], a robust control strategy providing seamless transition from islanded to grid-connected mode and vice versa of a grid-connected PV system is proposed. In grid-connected mode, the Advanced Robust Normalized Sign Shrinkage based control algorithm provides load reactive power compensation and harmonic elimination with unity power factor operation. In standalone mode, the resonant proportional controller and fast Fourier transform phase-locked loop ensure that the non-linear load is supplied with good quality voltage without interruption. In [40], a controller is proposed to provide both grid-connected and islanded mode. In this work in addition to the PV system, a battery and a diesel generator are used to minimize the fluctuation, help the microgrid ride-through the fault and controls the frequency and voltage in isochronous mode. In addition to the complexity of the system proposed by the authors, the study does not consider the elimination of harmonics on the grid side that could be caused by non-linear loads. An optimal coordinated performance strategy for power electronic converters under grid and island operating conditions for hybrid microgrid power management is proposed in [41]. Input-output feedback linearization and sliding mode controller (SMC) are implemented and proposed by the authors for this purpose. In this work, the PV system is considered as an independent power source that requires a grid synchronization strategy in connected mode and another control strategy in isolated mode to ensure the continuity of power supply to loads. The power quality aspect, including harmonic elimination, reactive power compensation and power factor improvement on the grid side in connected mode, is not considered in some cases and in others requires an additional active filter. All this makes the system complex.

In In this paper, a control strategy taking into account the islanded mode is proposed for the configuration where the PV system is connected to the grid through an active shunt power filter. A robust control of a PV-SAPF in islanding operation based on a new reference currents determination strategy is proposed. This control strategy will allow the PV system to perform the functions of partial or full load supply, harmonic elimination, low-THD current injection into the grid and to avoid damage to connected loads during islanding operation. The proposed strategy control is based on MVF harmonic identification method, which is independent of voltage grid, on the islanding detection algorithm, and on load shedding algorithm proposed of Kenfack *et* al. [42]. Based on the principle of optimal operating point tracking of PV system, it allows to remove the maximum power

extraction DC/DC converter. In summary, the two contributions of this work, are:

➢ The simplification of the PV-SAPF system structure achieved by removing the maximum power extraction DC/DC converter;

➢ The proposal of a control strategy to ensure the functioning of the system in case of islanding.

The remaining part of this paper is organized as follows: In section 2, the description of PV-SAPF system is done. Then, the control strategy proposed is described in section 3. The performance of control strategy proposed illustrated by numerical simulations in MATLAB/Simulink software are presented in section 4. Finally, section 5 concludes the paper.

## 2. Systems Modelling and Description

The system studied in this work is a PV-based SAPF, where the PV system is connected to the grid through a SAPF. In this configuration, the grid-connected inverter is controlled to allow the PV system to perform the functions of power quality, load supply and grid injection of low-THD current. In Fig. 1, the functional components are presented. The system consists of the PV system interfaced to the grid via a DC/AC converter, the control block, and the non-linear and linear loads. The reference currents of the grid-connected inverter are provided by the control strategy and the power switches control pulses by the sliding mode controller. The islanding block detects the disconnection from the grid and load shedding is used for load regulation in islanding operation in case of underproduction of the PV system. The adaptive algorithm is used to shift the operating point of the PV system.
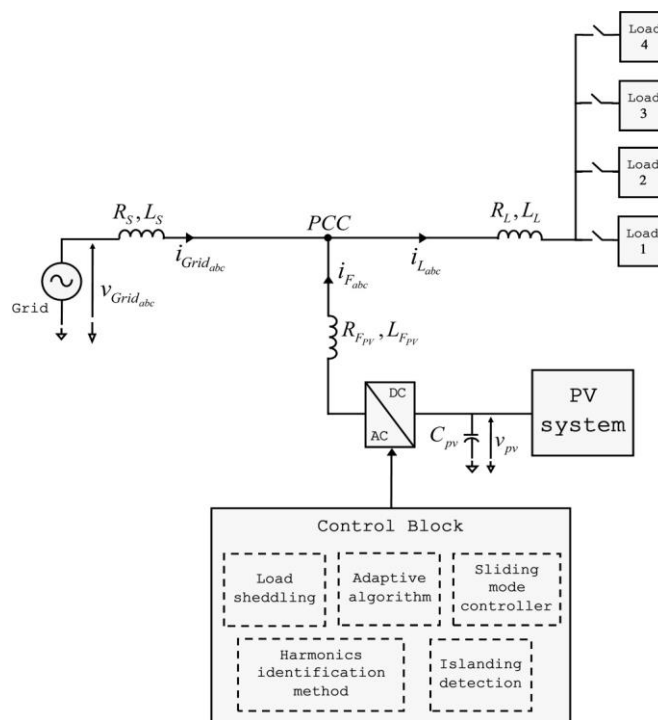


**Fig. 1.** Block diagram of PV-SAPF studied.

### 2.1. Modelling of the PV System

The PV system consists of several solar panels connected in series and/or parallel. Each panel consists of several cells connected in the same way. Fig. 2 shows the equivalent electrical circuit of a solar cell. Its consist of a perfect current source $I_{ph}$, in parallel with a diode $D$ and a shunt resistor $R_{Sh}$ crossed respectively by currents $I_D$ et $I_p$, the whole in series with a resistor $R_s$. The cell supplies the load with a current $I_{pv}$ at a voltage $V_{pv}$.
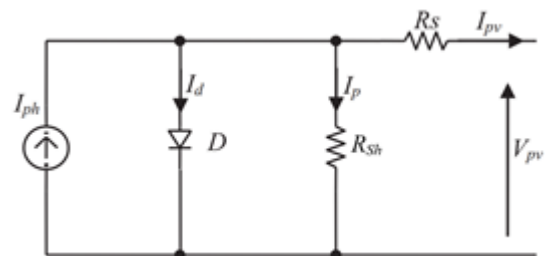


**Fig. 2.** Solar cell equivalent model [43].

The output current of solar cell is given by the following expression [43]:

$$I_{pv} = I_{ph} - I_s \left( \exp\left( \frac{q\left(V_{pv} + R_s I_{pv}\right)}{n K_b T} \right) - 1 \right) - \frac{V_{pv} + R_s I_{pv}}{R_{sh}} \quad (1)$$

With

$$I_{ph} = \left(\frac{G}{G_r}\right)\left(I_{scr} + k_i\left(T - T_r\right)\right)$$

$$I_S = I_{rs}\left(\frac{T}{T_r}\right)^3 \exp\left(\frac{qE_g}{nK_b}\left(\frac{1}{T_r} - \frac{1}{T}\right)\right)$$

$$I_{rs} = \frac{I_{scr}}{\exp\left(\frac{qV_{oc}}{nK_bT}\right) - 1}$$

Where

➢ $I_s$, $I_{rs}$ and $I_{scr}$ are respectively diode saturation current, diode saturation current at reference temperature and short-circuit current of PV module at standard test condition;

➢ $V_{pv}$ and $V_{oc}$ are respectively output voltage of PV cell and open-circuit voltage;

➢ $E_g$ is silicon gap energy of semiconductor;

➢ $T$ and $T_r$ are respectively cell and reference temperature;

➢ $G$ and $G_r$ are respectively solar and reference irradiation;

➢ $q$, $n$, $K_b$ and $k_i$ are respectively electron's charge, diode ideality coefficient, Boltzmann's constant and temperature coefficient of short-circuit.

For $N_S$ cells in series, and $N_P$ branches in parallel, the characteristic equation of a PV module is delivered as below [44]:

$$I_{pv} = N_p I_{ph} - N_p I_s\left(\exp\left(\frac{q\left(V_{pv} + R_s I_{pv}\right)}{N_s nK_b T}\right) - 1\right) - \frac{V_{pv} + R_s I_{pv}}{R_{sh}} \quad (2)$$

### 2.2. Modelling of a SAPF

The structure of two-level three-phase three-wire SAPF used in this paper is shown in Fig. 3. This structure consists of a three-phase, two-level inverter with 6 bi-directional power switches in current, a DC voltage source and a coupling filter serving as an interface between the DC/AC converter and the rest of the system.

The non-linear mathematical model can be described in the three-phase reference frame as follows [26]:

$$\begin{cases} L_F \dfrac{di_{Fa}}{dt} = -R_F i_{Fa} + v_{Fa} - v_{Grida} \\[2mm] L_F \dfrac{di_{Fb}}{dt} = -R_F i_{Fb} + v_{Fb} - v_{Gridb} \\[2mm] L_F \dfrac{di_{Fc}}{dt} = -R_F i_{Fc} + v_{Fc} - v_{Gridc} \end{cases} \quad (3)$$
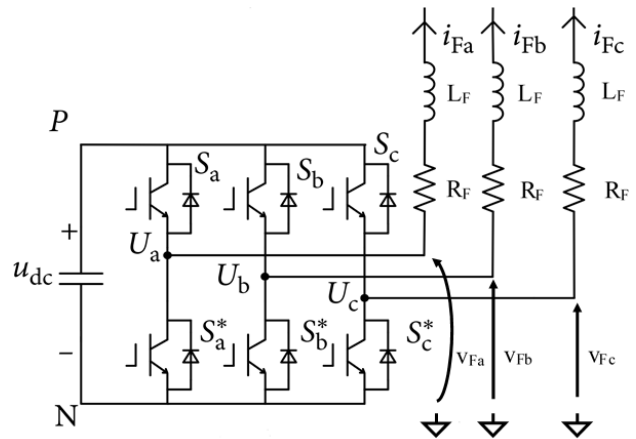


**Fig. 3.** SAPF structure [26].

In PV-SAPF configuration, the DC supplying is ensured by the PV system connected through a capacitor.

### 2.3. Control Block

The control block consists of the following elements:

➢ The harmonic identification method for reference currents components extraction;

➢ Sliding mode controller for the generation of switches control pulses of grid-connected inverter;

➢ The islanding block for detection of grid disconnection;

➢ Load shedding for load regulation in islanding operation in case of underproduction of the PV system;

➢ Adaptive algorithm for shifting the operating point of the PV system.

#### 2.3.1. Islanding Detection Method

The islanding detection method is based on the THD of the voltage at the PCC and the amplitude of grid current. Assuming that the grid is perfect and that only current harmonics are generated by the load, in normal operation the voltage at the PCC is perfectly sinusoidal with a THD close to 0%. In case of islanding this voltage is distorted and its THD increases considerably. The amplitude of the grid current is associated with the THD of the voltage at the PCC to make the algorithm robust. This amplitude is compared to an experimentally determined threshold value. Fig. 4 shows the proposed islanding algorithm.
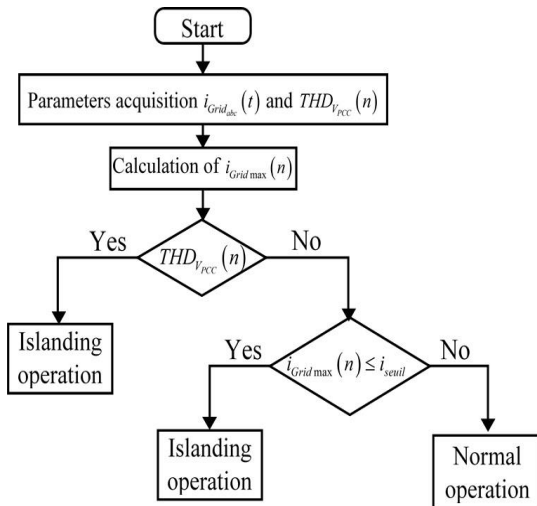
**Fig. 4.** Islanding detection method proposed.

### 2.1.1. Loads Shedding Method

The method of load shedding used in this paper is the one proposed in [42]. The loads shedding is used in case of underproduction of PV system in islanding operation. This method is based on the matches of apparent powers of loads with the one available in the PV system to determine the loads to be disconnected. The Fig. 5 shows the flow chart of loads shedding method for three loads.
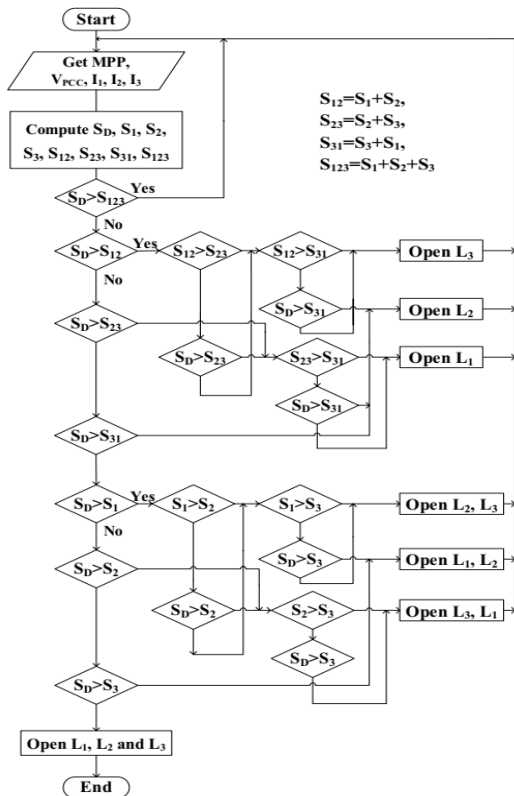


**Fig. 5.** Load shedding method [42].

In the flow chart of tmethod:

➤ $I_1$, $I_2$ and $I_3$ are the currents drawn by Loads 1, 2 and 3.

➤ $V_{PCC}$ is the voltage at the PCC.

➤ $S_1$, $S_2$, and $S_3$ are the apparent powers of loads 1, 2, and 3.

➤ $S_D$ is the apparent power produced by PV system.

## 3. Control Strategy Proposed

This section presents the principle of the proposed control strategy, its application with the MVF harmonic identification method and the proposed adaptive algorithm for shifting the PV system operating point. As the control of the SAPF is indirect, the sliding mode controller used is also presented.

### 3.1. Principle of the Strategy for Determining Reference Currents

The proposed control strategy is based on shifting the operational operating point of the PV system. The operating point of the PV system is chosen to find the best compromise between the production and the functions provided. For this purpose, reference currents of with two components, one, the harmonic component linked to the harmonics contained in the load current and the other, the fundamental component linked to the fundamental of the load current are generated. These reference currents are deduced from their harmonic and fundamental components according to the following equation:

$$i^* = i^*_{harm} + k_f i^*_{fund} \qquad (4)$$

Where

$i^*$ is the reference current, $i^*_{harm}$ is the harmonic component of reference current, $i^*_{fund}$ is the fundamental component of reference current, $k_f$ is the modulation coefficient of fundamental component.

The harmonic component of the reference current is the sum of the harmonic components of the load current. It is extracted from the load current using a harmonic identification method. This component is re-injected in phase opposition to the load current at the PCC to eliminate the harmonics generated by the load and thus, enable the PV system to perform with power quality function.

The fundamental component of the reference currents is the fundamental component of the load current. This component is re-injected in phase to the load current at the PCC to perform with load supply, low-THD current injection into the grid functions or both function. The modulation coefficient of the fundamental component can vary from 0 to infinity depending on the weather conditions.

The sum of the two components is used to impose an operating point on the PV system. This sum represents the reference signal for controlling the grid-connected inverter. The modulation coefficient of the fundamental component of the reference currents is done by an adaptive algorithm to minimize the THD of the currents injected into the grid or drawn from the grid by the load. Fig. 6 shows the block diagram of the proposed control strategy.
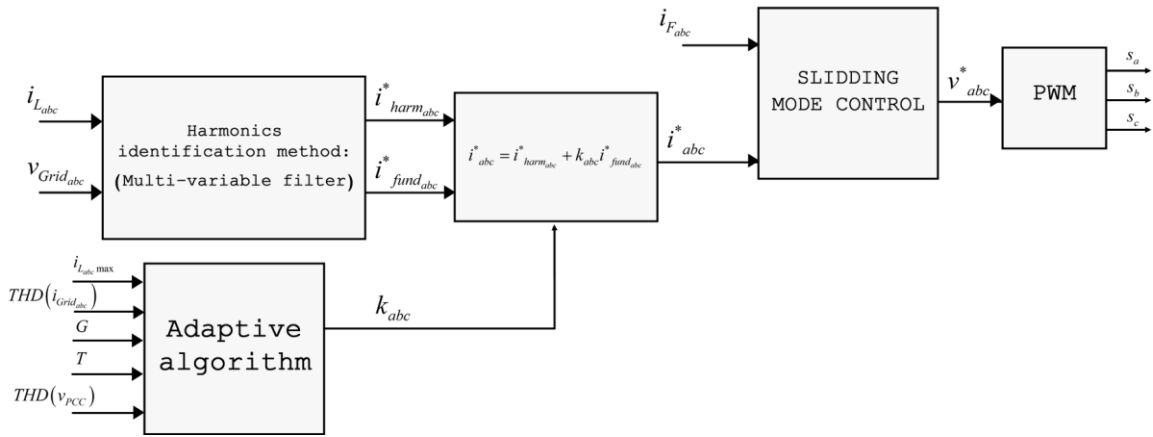
**Fig. 6.** Block diagram of the proposed control strategy for PV-SAPF system.

### 3.2. Harmonic Identification Method

The harmonic and fundamental components of the reference currents are determined using a harmonic identification method. Since island operation has to be taken into account, the MVF is used. This choice is justified by the fact that the identification of the components of the reference currents are independent of the network parameters. The MVF introduced by [45], is a new filter for extracting the fundamental component or other harmonic rank of electrical signals directly in Concordia reference frame. The transfer function of this filter is given by [46]:

$$H(s) = \frac{\hat{x}_{\alpha\beta}(s)}{x_{\alpha\beta}(s)} = K \frac{(s+K_c)+j\omega_c}{(s+K_c)^2+\omega_c^2} \qquad (5)$$

where

$\hat{x}_{\alpha\beta}(s)$ is the electrical output signal of MVF, $x_{\alpha\beta}(s)$ is the electrical input signal of MVF, $K_c$ is a positive constant and $\omega_c$ is the cut-off pulsation of MVF.

The cut-off pulsation of the filter is chosen to extract the fundamental component of the load current. The harmonic components are deduced by the difference between the load current and its fundamental component. The inputs to the MVF are the $(\alpha,\beta)$ components of the load current obtained by applying the Clarke transform to the three-phase load currents according to the following equation.

$$\begin{bmatrix} i_{L_\alpha} \\ i_{L_\beta} \end{bmatrix} = \sqrt{\frac{2}{3}} \begin{bmatrix} 1 & -\frac{1}{2} & -\frac{1}{2} \\ 0 & \frac{\sqrt{3}}{2} & -\frac{\sqrt{3}}{2} \end{bmatrix} \begin{bmatrix} i_{L_a} \\ i_{L_b} \\ i_{L_c} \end{bmatrix} \qquad (6)$$

The outputs to the MVF are the DC components $\bar{i}_{L\alpha}$ and $\bar{i}_{L\beta}$ linked to the fundamental and the AC components $\tilde{i}_{L\alpha}$ and $\tilde{i}_{L\beta}$ linked to the sum of harmonics. These DC and AC components represent respectively the fundamental and harmonic components of the reference currents. By inverse Clarke transformation, the three-phase components of the harmonic and fundamental components of the reference currents are given by the following equations:

$$\begin{bmatrix} i^*_{harm_a} \\ i^*_{harm_b} \\ i^*_{harm_c} \end{bmatrix} = \sqrt{\frac{2}{3}} \begin{bmatrix} 1 & 0 \\ -\frac{1}{2} & \frac{\sqrt{3}}{2} \\ -\frac{1}{2} & -\frac{\sqrt{3}}{2} \end{bmatrix} \begin{bmatrix} \tilde{i}_{L\alpha} \\ \tilde{i}_{L\alpha} \end{bmatrix} \qquad (7)$$

$$\begin{bmatrix} i^*_{fund_a} \\ i^*_{fund_b} \\ i^*_{fund_c} \end{bmatrix} = \sqrt{\frac{2}{3}} \begin{bmatrix} 1 & 0 \\ -\frac{1}{2} & \frac{\sqrt{3}}{2} \\ -\frac{1}{2} & -\frac{\sqrt{3}}{2} \end{bmatrix} \begin{bmatrix} \bar{i}_{L\alpha} \\ \bar{i}_{L\beta} \end{bmatrix} \qquad (8)$$

The reference currents are deduced from their harmonic and fundamental components according to the Eq. (4). The Fig. 8 illustrates the control strategy proposed for calculation of reference currents.

### 3.3. Synthesis of Robust Controller

The grid-inverter is controlled by sliding mode controller. This control strategy is based on the non-linear model of the filter. As one variable corresponds to one controller, the stationary filter model given in Eq. (9) is used for controller.

$$\begin{cases} L_F \dfrac{di_{F\alpha}}{dt} = -R_F i_{F\alpha} + v_{F\alpha} - v_{Grid\alpha} \\ L_F \dfrac{di_{F\beta}}{dt} = -R_F i_{F\beta} + v_{F\beta} - v_{Grid\beta} \end{cases} \qquad (9)$$

With

$$\begin{bmatrix} v_{F\alpha} \\ v_{F\beta} \end{bmatrix} = \sqrt{\frac{2}{3}} \begin{bmatrix} 1 & -\frac{1}{2} & -\frac{1}{2} \\ 0 & \frac{\sqrt{3}}{2} & -\frac{\sqrt{3}}{2} \end{bmatrix} \begin{bmatrix} v_{Fa} \\ v_{Fb} \\ v_{Fc} \end{bmatrix}$$

$$\begin{bmatrix} i_{F\alpha} \\ i_{F\beta} \end{bmatrix} = \sqrt{\frac{2}{3}} \begin{bmatrix} 1 & -\frac{1}{2} & -\frac{1}{2} \\ 0 & \frac{\sqrt{3}}{2} & -\frac{\sqrt{3}}{2} \end{bmatrix} \begin{bmatrix} i_{Fa} \\ i_{Fb} \\ i_{Fc} \end{bmatrix}$$

The sliding planes used are those proposed in [47] and given in Eq. (10).

$$\begin{cases} P(i_{F\alpha}) = k_1 e(i_{F\alpha}) + k_2 \int e(i_{F\alpha}) \\ P(i_{F\beta}) = k_3 e(i_{F\beta}) + k_4 \int e(i_{F\beta}) \end{cases} \quad (10)$$

where

➢ $e(i_{F\alpha}) = i_{Comp\alpha} - i_{F\alpha}$ is the error of the variable $i_{F\alpha}$

➢ $e(i_{F\beta}) = i_{Comp\beta} - i_{F\beta}$ is the error of the variable $i_{F\beta}$

➢ $k_1$, $k_2$, $k_3$ and $k_4$ positive constants.

The control laws are determined so that they verify the relations of Eq. (11) during the slip mode.

$$\begin{cases} P(i_{F\alpha,\beta}) = 0 \\ \dfrac{d}{dt} P(i_{F\alpha,\beta}) = 0 \end{cases} \quad (11)$$

By applying the conditions of Eq. (11) to the sliding planes of Eq. (10), the control laws are given by:

$$\begin{cases} v_{F\alpha\_ref} = \dfrac{k_2}{k_1} L_F e(i_{F\alpha}) + v_{Grid\alpha} + R_F i_{F\alpha} + L_F \dfrac{di_{Comp\alpha}}{dt} \\ v_{F\beta\_ref} = \dfrac{k_4}{k_3} L_F e(i_{F\beta}) + v_{Grid\beta} + R_F i_{F\beta} + L_F \dfrac{di_{Comp\beta}}{dt} \end{cases} \quad (12)$$
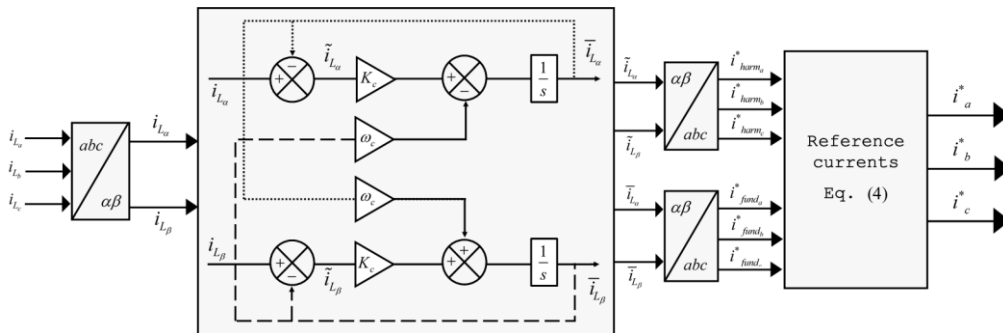


**Fig. 7.** Block diagram of determination of reference currents with MVF

### 3.4. Adaptive Algorithm

The adaptive algorithm used in the proposed control strategy, allows to shift the operating point of the PV system by modulating the value of the fundamental components of the reference currents. The modulation coefficients obtained at the output of the algorithm provide the following three functions:
➢ The injecting a low-THD current into the grid;
➢ Partially or fully supply the load;

➢ Ensure system operation in case of islanding.

The input parameters of the algorithm taken into account to calculate the modulation coefficients are the solar irradiation, the cell temperature, the maximum current of the load current, the THD of the grid current, and the islanding operation. The solar irradiation and cell temperature are used to estimate the maximum value of the PV system current. Fig. 9 shows the flow chart of the adaptive algorithm of the proposed control strategy.
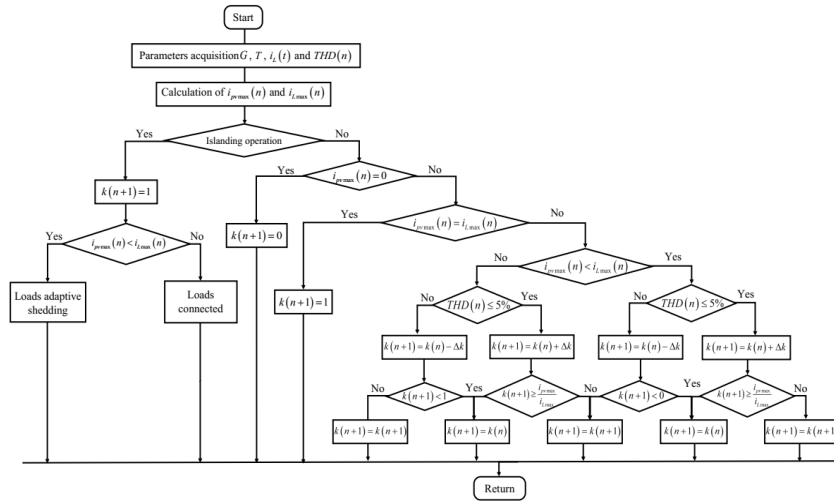
**Fig. 8.** Flow chart of adaptive algorithm

## 4. Results and Discussions

The effectiveness of the proposed control strategy is evaluated in this section by numerical simulations in Matlab/Simulink software, using the fixed-step time ODE3 (Bogacki-Shampine) solver and the Simpower system toolbox. The simulation parameters of the grid, the grid-connected inverter, the MVF, the SMC, the adaptive algorithm and the PV system are given in Table 1 at 6 respectively.

**Table 1.** Grid parameters

| Name | Symbols | Values | unity |
|------|---------|--------|-------|
| Voltage | $V_{RMS}$ | 230 | V |
| Frequency | $f_S$ | 50 | Hz |
| Resistance | $R_S$ | 3.5 | mΩ |
| Inductance | $L_S$ | 0.023 | mH |

**Table 2.** Grid-connected inverter parameters

| Name | Symbols | Values | unity |
|------|---------|--------|-------|
| Capacitance | $C_{pv}$ | 100 | µF |
| Resistance | $R_f$ | 23 | mΩ |
| Inductance | $L_f$ | 3 | mH |

**Table 3.** MVF parameters

| Name | Symbols | Values | unity |
|------|---------|--------|-------|
| Positive constant | $K_C$ | 50 | |
| Cut-off pulsation | $\omega_S$ | $100\pi$ | Rad/s |

**Table 4.** Adaptive algorithm parameters

| Name | Symbols | Values | unity |
|------|---------|--------|-------|
| measurement interval | $\Delta t$ | 0.025 | s |
| Increment value | $\Delta k$ | 0.1 | |

**Table 5.** SMC parameters

| Symbols | Values |
|---------|--------|
| $k_1$ | 1e-5 |
| $k_2$ | 5e5 |
| $k_3$ | 1e-5 |
| $k_4$ | 5e5 |

**Table 6.** PV system parameters

| Name | Symbols | Values | unity |
|------|---------|--------|-------|
| Cells per module | $N_{Cell}$ | 128 | |
| Maximum power | $P_m$ | 414.801 | W |
| Voltage at PPM | $V_{MPP}$ | 72.9 | V |
| Current at PPM | $I_{MPP}$ | 5.69 | A |
| Open circuit voltage | $V_{OC}$ | 85.3 | V |
| Short-circuit current | $I_{SC}$ | 6.09 | A |
| Diode ideality factor | $n$ | 0.87223 | |
| Shunt resistance | $R_{Sh}$ | 419.7813 | Ω |
| Series resistance | $R_S$ | 0.5371 | Ω |
| Temperature coefficient of $V_{oc}$ | $k_v$ | -0.229 | %/deg.C |
| Temperature coefficient of $I_{sc}$ | $k_i$ | 0.030706 | %/deg.C |
| Panel in series | $N_S$ | 10 | |
| Panel in parallel | $N_P$ | 20 | |

To illustrate the performances of the proposed control strategy, the following operating scenarios are simulated.

➤ Renewable overproduction scenario with islanding;

➤ Renewable underproduction scenario with islanding.

### 4.1. Renewable Overproduction Scenario with Islanding

In this section, the power produced by the PV system is higher than that required by all loads. Two loads are used in this scenario, one linear and one non-linear. Non-linear load is a three-phase bridge rectifier supplying a resistor $R = 10\Omega$ in series with an inductor $L = 2.6mH$ and the linear load is a three-phase resistor $R = 22\Omega$. The linear load is connected

during the simulation from 0.5s. The solar irradiation and temperature are fixed respectively at $1000W/m^2$ and $25°C$ .
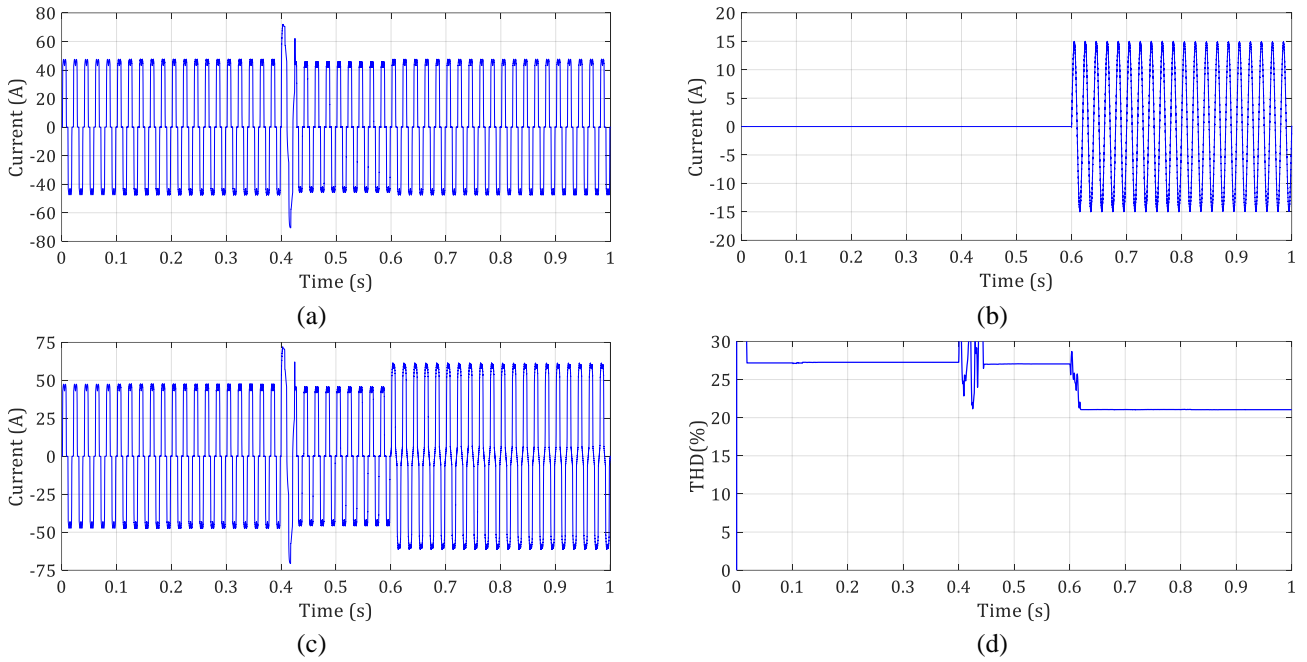


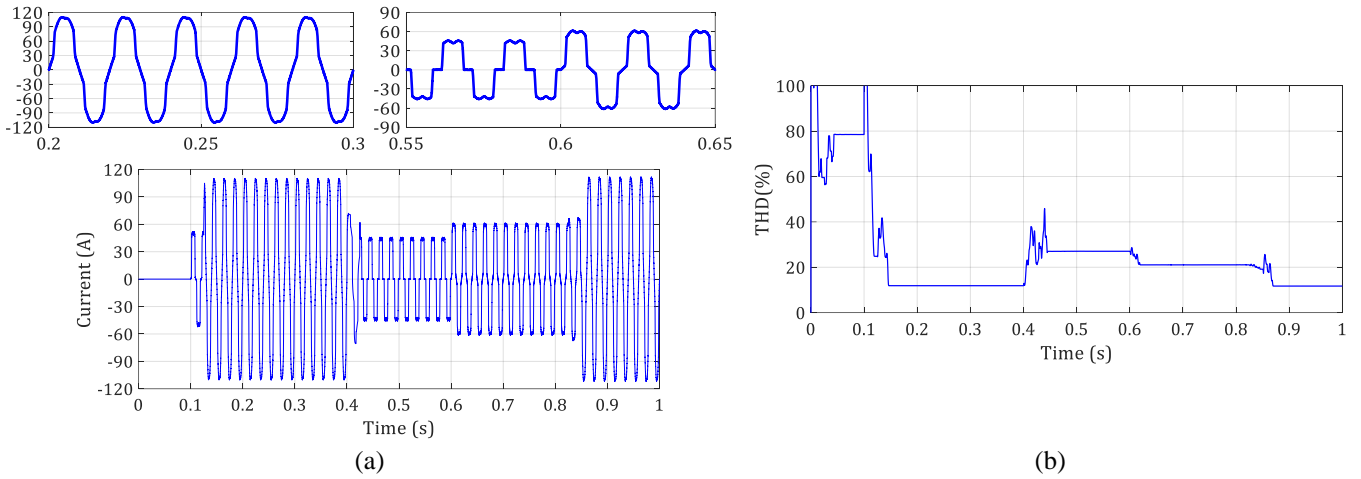**Fig. 9.** Non-linear load current (a), linear load current (b), total load current (c) and its THD (d)



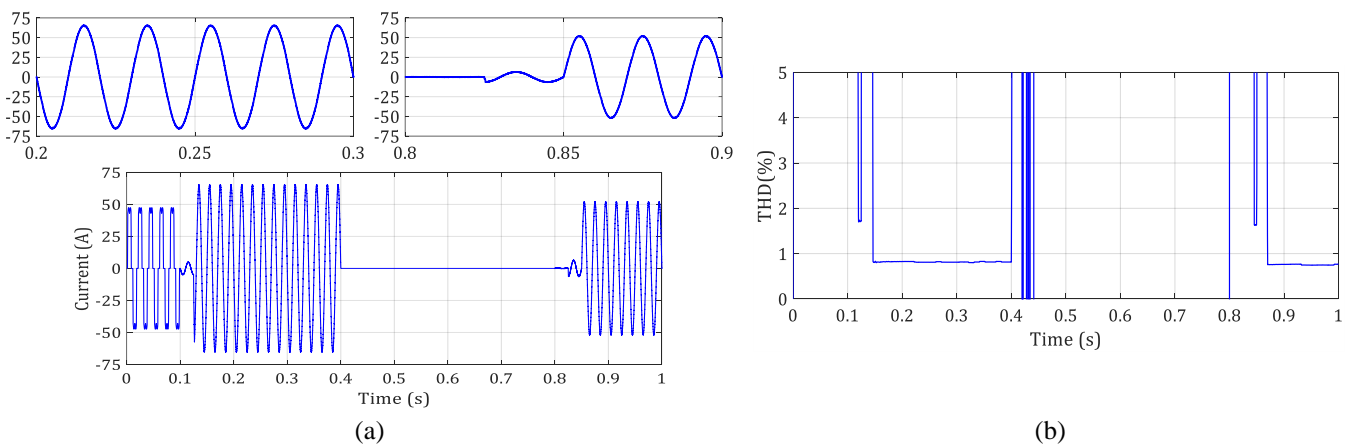**Fig. 10.** Filter current injected by PV system (a) and its THD (b)
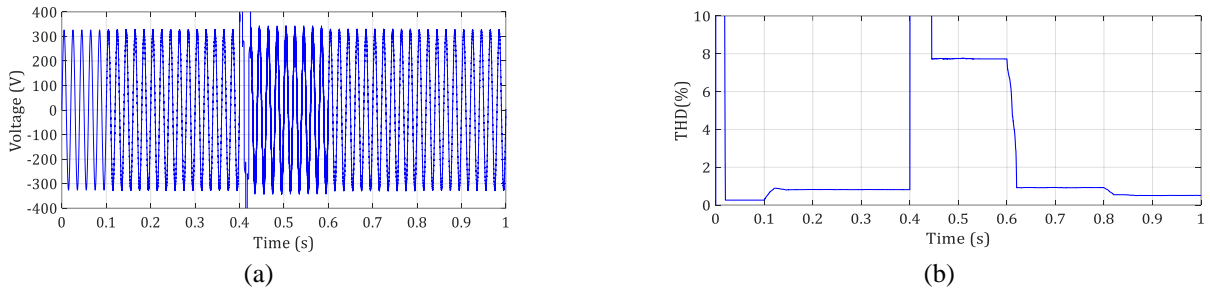


**Fig. 11.** Grid current (a) and its THD (b)

(a)　　　　　　　　　　　　　　　　　　　　(b)

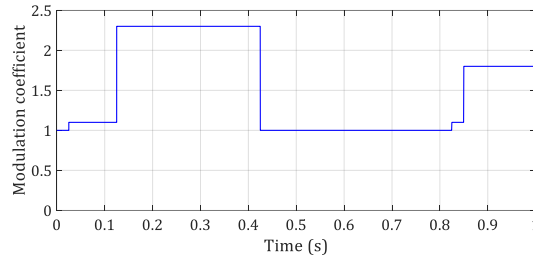**Fig.12.** Voltage at the PCC (a) and its THD (b)



**Fig. 13.** Modulation coefficient

Before islanding, i.e. between 0s and 0.4s, the PV system alone provides the power required by the load and injects a sinusoidal waveform current into the grid with a low THD of less than 1%. This can be seen in Figures 10(a) and 10(b), which show the waveform and THD of the grid current respectively. In this phase, the PV system performs its functions of load supply and low THD current injection into the grid. Indeed, in this phase, the modulation coefficients of the fundamental components of the reference currents are equal to 2.3, which means that 1.3 times the fundamental value of the load current is injected into the grid (see Fig 11).

During islanding, which occurs between 0.4s and 0.8s, the deterioration of the voltage waveform at the PCC leads to an increase in its THD from a value close to 0% to a value above the set threshold value of 5%. In addition, the amplitude of the grid current becomes lower than the set threshold value. These two observations, which can be seen in Fig. 12 and 13, are analyzed by the islanding algorithm, which sends back to the adaptive algorithm the information that the grid has disconnected. The absence of the grid leads the adaptive algorithm to impose the value of the modulation coefficient to 1, which is interpreted by the cancellation of the low THD current injection function in the grid, to satisfy only the load supply function. During this islanding phase, the current supplied by the filter is identical to that required by the load with the same waveform and THD value (see Fig. 9(c), 9(d), 10(a) and 10(b)). Connecting an additional linear load during islanding does not change the performance of the control strategy, which simply updates the operating point position of the PV system corresponding to the new required load current. Figures 9(a) and 9(b) show the current waveforms of the non-linear load and the additional linear load.

After islanding, i.e. between 0.8s and 1.0s, with the grid connected again, the PV system performs its function of injecting low THD current into the grid again. The operating point of the PV system is changed again by the adaptive algorithm, which increases the modulation coefficient from 1 to 1.8. The PV system alone provides the power required by the load and injects a current with a THD of less than 1% into the grid (see Fig. 11).

### 4.2. Renewable Underproduction Scenario with Islanding

In this section, the power produced by the PV system is lower than that required by all loads. Four loads are used in this scenario, one non-linear and three linears. Non-linear load is a three-phase bridge rectifier supplying a resistor $R = 10\Omega$ in series with an inductor $L = 2.6mH$ and the linear loads are of three-phase resistors of values $R = 47\Omega$, $R = 33\Omega$ and $R = 10\Omega$ respectively. The solar irradiation and temperature are fixed respectively at $600W/m^2$ and $25°C$.

Before islanding, i.e. between 0s and 0.4s, the modulation coefficient stabilizes at a value of 0.7. This value being between 0 and 1, it means that the PV system supplies the load partially, and eliminates the harmonics produced by the load on the grid side. As the grid provides part of the power required by the load, the load draws a distorted current from the grid which is made sinusoidal by the action of the filter. The THD of the grid current therefore falls from a value of 15% (in the absence of the 0s - 0.1s filter) to a value of less than 0.5%. In this phase, the PV system performs its functions of partial load supply and harmonic elimination.

During islanding, which occurs between 0.4s and 0.8s, the deterioration of the voltage waveform at the PCC leads to an increase in its THD from a value close to 0% to a value above the set threshold value of 5%. In addition, the amplitude of the grid current becomes lower than the set threshold value. These two observations, which can be seen in Fig. 16 and 17, are analyzed by the islanding algorithm, which sends back to the adaptive algorithm the information

that the grid has disconnected. The absence of the grid leads the adaptive algorithm to impose the value of the modulation coefficient to 1. As the PV system is underproduction, the

load shedding algorithm comes into play in order to have an overproduction scenario of the renewable source. With the load 4 disconnected, the current supplied by the filter become
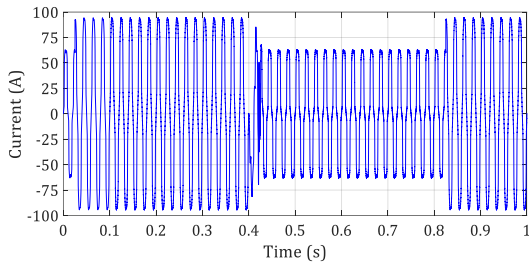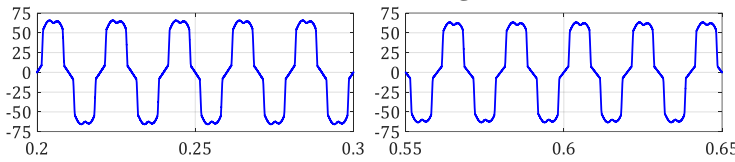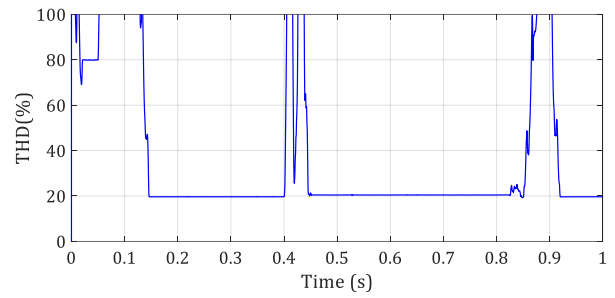


(a)
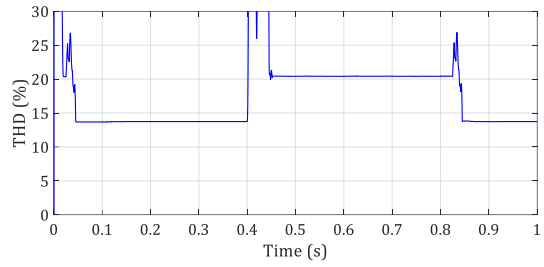
(b)

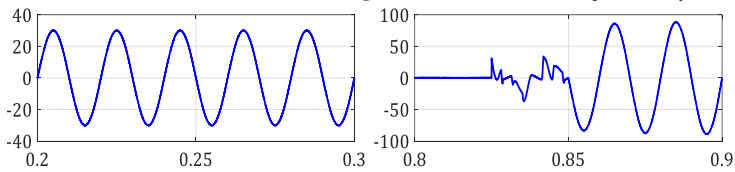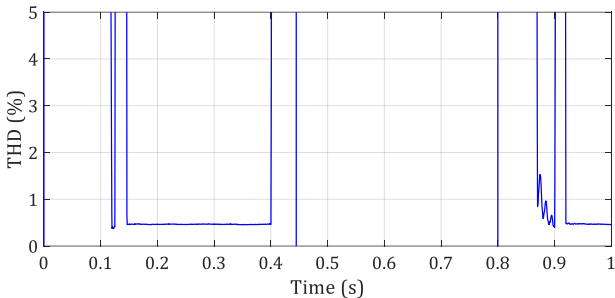**Fig. 14.** Total load current (a) and its THD (b)



(a)

(b)

**Fig. 15.** Filter current injected by PV system (a) and its THD (b)
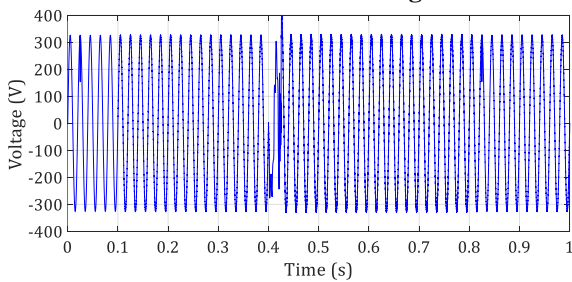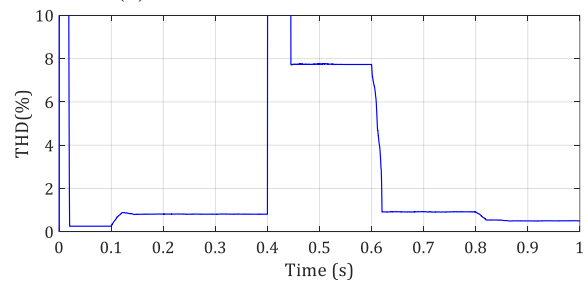


(a)

(b)

**Fig. 16.** Grid current (a) and its THD (b)



(a)

(b)

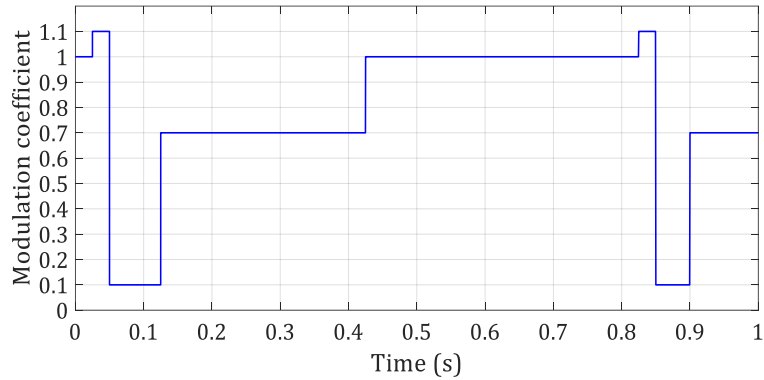**Fig. 17.** Voltage at the PCC (a) and its THD (b)

**Fig. 18.** Modulation coefficient

identical to the one required by the load with the same waveform and the same value of THD (see Fig. 14(a), 14(b), 15(a) and 15(b)).

After islanding, i.e. between 0.8s and 1.0s, with the grid connected again, the PV system performs its function of harmonics elimination again. The operating point of the PV system is changed again by the adaptive algorithm, which decreases the modulation coefficient from 1 to 0.7. The PV system provides partially the power required by the load and

eliminates the harmonics produced by the load on the grid side (see Fig. 16).

Table 7 and Table 8 below summarize the performance obtained in the two scenarios in terms of the function performed by the PV system, the THD of the grid and the response time following grid disconnection and reconnection: Table 7 for renewable overproduction scenario with islanding and Table 8 for renewable underproduction scenario with islanding.

**Table 7.** Performance indicators for scenario 1

| | | Before islanding | During islanding | After islanding |
|---|---|---|---|---|
| PV function (s) | | ➢ Total loads supply<br>➢ Low-THD current injection into the grid | Loads supply | ➢ Total loads supply<br>➢ Low-THD current injection into the grid |
| THD | Load | 27% | 27% | 27% |
| | Grid | 0.8% | / | 0.75% |
| Control response time | | 0.04s | / | 0.06s |

**Table 8.** Performance indicators for scenario 2

| | | Before islanding | During islanding | After islanding |
|---|---|---|---|---|
| PV function (s) | | ➢ Partially loads supply<br>➢ Harmonics elimination | Loads supply | ➢ Partially loads supply<br>➢ Harmonics elimination |
| THD | Load | 13.75% | 20.45% | 13.75% |
| | Grid | 0.47% | / | 0.47% |
| Control response time | | 0.05s | / | 0.12s |

From these two performance summary tables, it can be seen that before and after islanding, the control strategy allows the PV system to perform its functions of load supply (partially or fully), and power quality by injecting a low THD current into the grid or by eliminating harmonics created by the load on the grid side. During islanding, the PV system supplies the load. In the overproduction scenario, the problem caused by the lack of the grid into which the excess production was being injected is solved by shifting the operating point of the PV system to that of the load. In the underproduction scenario, the problem caused by the lack of the grid that was partially supplying the load is solved by shifting the operating point of the PV system followed by load shedding.

## 5. Conclusion

In this paper, the robust control of a PV-SAPF system with islanding operation is proposed. This control is based on a new strategy to determine the reference currents of the grid-connected inverter. The principle of this strategy is to provide reference currents of with two components, one, the harmonic component linked to the harmonics contained in the load current and the other, the fundamental component linked to the fundamental of the load current. The harmonic component enables the PV system to perform the power quality function, and the fundamental component enables the PV system to perform the load supply and low-THD current

injection into the grid. The combination of these two components allows the RES to perform the functions of partial or full load supply, power quality, low-THD current injection into the grid and to avoid damage to connected loads during islanding operation. In order to perform these different weather-dependent functions, an adaptive algorithm based on the energy produced by the PV system, the current consumed by the load and the THD of the grid current is used to modulate the fundamental components of the reference currents. This modulation of the value of the fundamental component makes it possible to impose an optimal operating point on the PV system, ensuring that it injects a low THD current into the grid, supplies the load partially or totally and ensures the operation of the system in case of islanding.

Different operating scenarios were simulated using MATLAB/Simulink software, and from the results obtained, the following contributions can be noted:

➢ In terms of structure, the proposed control strategy allows the removal of the maximum power extraction converter;

➢ In terms of effectiveness, the control strategy proposed allows:

o In case of overproduction of the photovoltaic system, that it supplies the load alone and injects into the grid a current with THD values lower than 1%;

o In case of underproduction of the photovoltaic system, that it contributes partially to the supply of the load and eliminates the harmonics on the grid side with THD values of the grid current lower than 0.5%;

o Ensure system operation in case of islanding.

A study for an unbalanced three-phase load and an experimental study to validate the theoretical results are the interesting perspectives to test the performance of the proposed control strategy.

**References**

[1] B. B. Adetokun, J. O. Ojo, and C. M. Muriithi, "Application of large-scale grid-connected solar photovoltaic system for voltage stability improvement of weak national grids", Scientific Reports, Vol. 11, pp. 1-15, December 2021.

[2] K. Dmitruk, and A. Sikorski, "Implementation of the Improved Active Frequency Drift Anti-Islanding Method into the Three-Phase AC/DC Converter with the LCL Grid Filter", Energy Reports, Vol. 7, pp. 1-14, February 2022.

[3] V. G. Gormo, D. K. Kidmo, B. P. Ngoussandou, B. Bogno, D. Raidandi, and M. Aillerie, "Wind power as an alternative to sustain the energy needs in Garoua and Guider, North Region of Cameroon", Energies, Vol. 15, pp. 814-829, May 2021.

[4] A. Adel, A. Elgammal, and F. Mohammed, E. naggar, "MOPSO-based optimal control of shunt active power filter using a variable structure fuzzy logic sliding mode controller for hybrid (FC-PV-Wind-Battery) energy utilisation scheme", IET Renewable Power Generation, Vol. 11, pp. 1148-1156, February 2017.

[5] Report IEA-PVPS T1-41, Trends in Photovoltaic Applications, International Energy Agency, 2021.

[6] A. Ouai, L. Mokrani, M. Machmoum, and A. Houari, "Control and energy management of a large scale grid-connected PV system for power quality improvement", Solar Energy, Vol. 171, pp. 893–906. September 2018.

[7] R. Belaidi, M. Hatti, A. Haddouche, M. M. Larafi, "Shunt active power filter connected to a photovoltaic array for compensating harmonics and reactive power simultaneously", 4th International Conference on Power Engineering, Energy and Electrical Drives, Istanbul, pp. 1482-1486, October 2013.

[8] U. K. Das, K. S. Tey, M. Seyedmahmoudian, S. Mekhilef, M. Y. Idna Idris, W. V. Deventer, B. Horan, and A. Stojcevski, "Forecasting of photovoltaic power generation and model optimization: A review", Renewable and Sustainable Energy Reviews, Vol. 81, pp. 912-928, January 2018.

[9] Y. Yu, M. Wang, F. Yan, M. Yang, and J. Yang, "Improved convolutional neural network-based quantile regression for regional photovoltaic generation probabilistic forecast", IET Renewable Power Generation, Vol. 14, pp. 2712-2719, October 2020.

[10] M. J. P. Pesdjock, J. R. Mboupda Pone, D. Tchiotsop, M. R. Douanla, and G. Kenne, "Minimization of currents harmonics injected for grid connected photovoltaic systems using duty-cycle modulation technique", International Journal of Dynamics and Control, Vol. 9, pp. 1013-1023, October 2020.

[11] Ndongmo Fotsa, S. Perabi Ngoffe, S. Ndjakomo Essiane, and G. Abessolo Ondoua, "Parameter Estimation of the Photovoltaic System Using Bald Eagle Search (BES) Algorithm", International Journal of Photoenergy, Vol. 2021, October 2021.

[12] F. Fissou Amigue, S. Ndjakomo Essiane, S. Perabi Ngoffe, and G. Abessolo Ondoa, G. Mengata Mengounou, P.T. Nna Nna, "Optimal integration of photovoltaic power into the electricity network using Slime mould algorithms: Application to the interconnected grid in North Cameroon", Energy Reports, Vol. 7, pp. 6292-6307, November 2021.

[13] D. Icaza, J. R. Espinoza, and D. Valarezo, "Study of a Hybrid System Wind-Photovoltaic on grid for The Self-Supply of Energy to an Area with Bioecological Infrastructure", 2021 9th International Conference on Smart Grid (icSmartGrid), Setubal, Portugal, pp. 264–272, 29 June - 01 July 2021.

[14] O. Guenounou, A. Belkaid, I. Colak, B. Dahhou, and F. Chabour, "Optimization of Fuzzy Logic Controller Based Maximum Power Point Tracking Using

Hierarchical Genetic Algorithms", 2021 9th International Conference on Smart Grid (icSmartGrid), Setubal, Portugal, pp. 207–211, 29 June - 01 July 2021.

[15] R. Balamurugan, and R. Nithya, "Solar PV Based Shunt Active Filter with p-q Theory Control for Improvement of Power Quality", Journal of Circuits, systems and computers, Vol. 26, pp. 1-13, 2017.

[16] R. Kitmo, D. Djidimbélé, D. Kaoga Kidmo, G. B. Tchaya, N. Djongyang, "Optimization of the power flow of photovoltaic generators in electrical networks by MPPT algorithm and parallel active filters", Energy Reports, Vol. 7, pp. 491-505, November 2021.

[17] A. Yousfi, A. Tayeb, and A. Chaker, "Power Quality Improvement Based on Five-Level Shunt APF Using Sliding Mode Control Scheme Connected to a Photovoltaic", International Journal of Smart Grid, Vol. 1, pp. 9-15, December 2017.

[18] J. Vaquero, N. Vázquez, I. Soriano, and J. Vázquez, "Grid-Connected Photovoltaic System with Active Power Filtering Functionality", International Journal of Photoenergy, Vol. 2018, Article ID 2140797, 9 pages, 2018.

[19] S. Torabi Jafrodi, M. Ghanbari, M. Mahmoudian M, A. Najafi, Eduardo M. G. Rodrigues, and E. Pouresmaeil, "A Novel Control Strategy to Active Power Filter with Load Voltage Support Considering Current Harmonic Compensation", Applied Sciences, Vol. 10, pp. 1-18, March 2020.

[20] Y. Hoon, M. A. M. Radzi, M. A. A. Mohd Zainuri, and Mohamad A. M. Zawawi, "Shunt Active Power Filter: A Review on Phase Synchronization Control Techniques", Electronics, Vol. 8, pp. 1-20, July 2019.

[21] IEEE Std 519-2014, IEEE Recommended Practice and Requirements for Harmonic Control in Electric Power Systems, The Institute of Electrical and Electronics Engineers, 2014.

[22] D. Buła, D. Grabowski, and M. Maciążek, "A Review on Optimization of Active Power Filter Placement and Sizing Methods", Energies, Vol. 15, pp. 1-35, February 2022.

[23] A. G. Lange, and G. Redlarski, "Selection of C-type filters for reactive power compensation and filtration of higher harmonics injected into the transmission system by arc furnaces", Energies, Vol. 13, pp. 1-19, May 2020.

[24] M. A. Moftah, G. El-Saady, and El-Noby A. Ibrahim, "Active Power Filter for Power Quailty Enhancement of Photovoltaic Renewable Energy Systems", Journal of Electrical Engineering, Vol. 17, pp. 1-9, March 2017.

[25] A. Bouhouta, S. Moulahoum, N. Kabache, and I. Colak, "Simplicity and Performance of Direct Current Control DCC Compared with other Identification Algorithms for Shunt Active Power Filter", 2018 7th International Conference on Renewable Energy Research and Applications (ICRERA), Paris, France, pp. 1352–1357, 14-17 October 2018.

[26] S. R. Das, P. K. Ray, A. K. Sahoo, S. Ramasubbareddy, T. S. Babu, N. M. Kumar, R. M. Elavarasan, and L. Mihet-Popa, "A Comprehensive Survey on Different Control Strategies and Applications of Active Power Filters for Power Quality Improvement", Energies, Vol. 14, pp. 1-32, July 2021.

[27] S. Ye, Y. Zhang, L. Xie, H. Lu, "Shunt Active Power Filter Based on Proportional Integral and Multi Vector Resonant Controllers for Compensating Nonlinear Loads", Journal of Electrical and Computer Engineering, 2018.

[28] R. Noroozian, and B. Gevorg Gharehpetian, "An investigation on combined operation of active power filter with photovoltaic arrays", International Journal of Electrical Power & Energy Systems, Vol. 46, pp. 392-399, March 2013.

[29] N. D. Tuyen, and G. Fujita, "PV-Active Power Filter Combination Supplies Power to Nonlinear Load and Compensates Utility Current", IEEE Power and Energy Technology Systems Journal, Vol. 2, pp. 32-42, June 2015.

[30] B. E. Youcefa, A. Massoum, S. Barkat, S. Bella, and P. Wira, "DPC Method For Grid Connected Photovoltaic System Acts as a Shunt Active Power Filter Implemented with Processor in the Loop", 2018 International Conference on Electrical Sciences and Technologies in Maghreb (CISTEM), Algers, pp 1-7, 28-31 October 2018.

[31] A. Benzahia, R. Boualaga, A. Moussi, L. Zellouma, M. Meriem, and B. Chaima, "A PV powered shunt active power filter for power quality improvement", Global Energy Interconnection, Vol. 2, pp. 143–149, April 2019.

[32] M. Jauhari, D. C. Riawan, and M. Ashari, "Control Design For Shunt Active Power Filter Based On p-q Theory In Photovoltaic Grid-Connected System", International Journal of Power Electronics and Drive Systems, Vol. 9, pp. 1064–1071, September 2018.

[33] S. Saidi, R. Abbassi, W. B. Hassen, and S. Chebbi, "Solar photovoltaic energy system-based shunt active filter for electrical energy quality improvement", International Journal of Simulation and Process Modelling, Vol. 11, pp. 119–126, June 2016.

[34] S. Krishna Kumar, J. Ranga, Ch. S. K. B. Pradeep, and S. Jayalakshmi, "PV based Shunt Active Power Filter for harmonics mitigation using Decoupled DSRF theory", 5th International Conference on Advanced Computing Communication Systems (ICACCS), Coimbatore, pp. 1108–1110, 15-16 March 2019.

[35] A. Azzam-Jai, and M. Ouassaid M, "A Multifunctional PV-Based Shunt Active Power Filter Using Neural Network Controller" International Symposium on Advanced Electrical and Communication Technologies (ISAECT), Rabat, pp 1-6, 2018.

[36] M. A. A. Mohd Zainuri, M. A. Mohd Radzi, A. Che Soh, N. Mariun, N. Abd Rahim, J. Teh, C.-M. Lai, "Photovoltaic Integrated Shunt Active Power Filter with Simpler ADALINE Algorithm for Current Harmonic Extraction", Energies, Vol. 11, pp. 1-22, May 2018.

[37] R. Kumar, H. O. Bansal, and H. P. Agrawal, "Development of fuzzy logic controller for photovoltaic integrated shunt active power filter", Journal of Intelligent & Fuzzy Systems, Vol. 36, pp. 6231-6243, June 2019.

[38] K. Barra, and D. Rahem, "Predictive direct power control for photovoltaic grid connected system: An approach based on multilevel converters", Energy Conversion and Management, Vol. 78, pp. 825-834, February 2014.

[39] S. Singh, S. Kewat, B. Singh, B. Ketan Panigrahi, and M. Kumar Kushwaha, "Seamless control of solar PV grid interfaced system with islanding operation", IEEE Power and Energy Technology Systems Journal, Vol. 6, pp. 162–171, September 2019.

[40] M. Y. Worku, M. A. Hassan, and M. A. Abido, "Real Time Energy Management and Control of Renewable Energy based Microgrid in Grid Connected and Island Modes", energies, Vol. 12, pp. 515–525, January 2019.

[41] Y. Toghani Holari, S. Abbas Taher, and M. Mehrasa, "Power management using robust control strategy in hybrid microgrid for both grid-connected and islanding modes, Journal of Energy Storage", Journal of Energy Storage, Vol. 39, pp. 102600, July 2021.

[42] S. R. Dzonde Naoussi, S. Kenfack Tsobze, and G. Kenne, "A new approach for islanding management in PV system using frequency modulation technique and simple adaptive load shedding algorithm", Springer Nature Applied Sciences, Vol. 2, pp. 583–590, November 2019.

[43] K. Tsamaase, J. Sakala, E. Rakgati, I. Zibani, and K. Motshidisi, "Solar PV Module Voltage Output and Maximum Power Yearly profile using Simulink-based Model", 2021 10th International Conference on Renewable Energy Research and Application (ICRERA), Istanbul, Turkey, pp. 31–35, 26-29 September 2021.

[44] F. E. Ndi, S. Ngoffe Perabi, S. Essiane Ndjakomo, G. Ondoua Abessolo, G. Mengounou Mengata, "Estimation of single-diode and two diode solar cell parameters by equilibrium optimizer method", Energy Reports, Vol. 7, pp. 4761-4768, November 2021.

[45] M. Abdusalam "Structures and strategies for control of parallel and hybrid active filters with experimental validations", 2008. PhD Thesis Henri Poincaré University, Nancy-1, France

[46] G. Pathak, D. Mohanty, S. K. Dwivedi, B. Singh, B. K. Panigrahi, "Implementation of MVF-Based Control Technique for 3-Φ Distribution Static Compensator. Journal of the Institution of Engineers India Series B, Vol. 100, pp. 589–597, 2019.

[47] R. C. Fanjip, S. R. Dzonde Naoussi, C. H. Kom, A. Nanfak, and G. M. Ngaleu, "Fuzzy sliding mode control of a shunt active power filter for harmonic reduction in grid-connected photovoltaic systems," Journal of Electrical Engineering, Electronics, Control and Computer Science, Vol. 8, pp. 43-54, January 2022.